Radiative lifetimes of dipolar excitons in double quantum wells

Yotam Mazuz-Harpaz, Kobi Cohen, Boris Laikhtman, Ronen Rapaport, Ken West, and Loren N. Pfeiffer

Phys. Rev. B **95**, 155302 — Published 4 April 2017

DOI: 10.1103/PhysRevB.95.155302

Radiative Lifetimes of Dipolar Excitons in Double Quantum-Wells

Yotam Mazuz-Harpaz, Kobi Cohen, Boris Laikhtman, and Ronen Rapaport
Racah Institute of Physics, The Hebrew University of Jerusalem, Jerusalem 9190401, Israel.

Ken West and Loren N. Pfeiffer
Department of Electrical Engineering, Princeton University, Princeton, New Jersey 08544, USA.
(Dated: March 13, 2017)

Spatially indirect excitons in semiconducting double quantum wells have been shown to exhibit rich collective many-body behavior that result from the nature of the extended dipole-dipole interactions between particles. For many spectroscopic studies of the emission from a system of such indirect excitons, it is crucial to separate the single particle properties of the excitons from the many-body effects arising from their mutual interactions. In particular, knowledge of the relation between the emission energy of indirect excitons and their radiative lifetime could be highly beneficial for control, manipulation, and analysis of such systems. Here we study a simple analytic approximate relation between the radiative lifetime of indirect excitons and their emission energy. We show, both numerically and experimentally, the validity and the limits of this approximate relation. This relation between the emission energy and the lifetime of indirect excitons can be used to tune and determine their lifetime and their resulting dynamics without the need of directly measuring it, and as a tool for design of indirect exciton based devices.

I. INTRODUCTION

An indirect exciton (IX) is a coulomb-bound complex of an electron (e) and a hole (h) where the opposite charges of the bound complex are spatially separated in two parallel layers with a tunneling barrier between them, as is depicted in Fig. 1. Such IXs are usually formed by optical excitation of an electrically biased double quantum well (DQW) heterostructure[1–3]. This spatial e-h separation leads to a long radiative lifetime and to a large electrical dipole moment of the IX. Due to the combination of these two properties, IXs give a unique opportunity to observe and study interesting cold interacting low-dimensional fluids.

In recent years, an intensive experimental and theoretical effort focused on IX fluids in GaAs based DQWs revealed many intriguing phenomena, such as spontaneous pattern formation[4–7], spin textures[8], interaction-induced particle correlations[9,10], molecular IX complexes[11,12], as well as evidence for complex collective phases[10,13–17]. On the other hand, recent progress in the techniques for control and manipulation of IXs led to demonstration of various kinds of complex device functionalities such as trapping schemes[11,18–21], flow control, IX transport and routing[22–26], and spin transport[27,28]. Due to these recent advancements, cold IX fluids started attracting the interest of a wider scientific community, and new experiments on dipolar fluids of IXs in newly emerging systems have been performed recently. These include bilayer two-dimensional transition metal DiChalcagonide systems[29,30], bilayer graphene[31,32] and polaritonic systems[33–36] among others.

To fully understand and control the various properties of such optically generated IX fluids, it is very important to have a good insight on their intrinsic dynamics. A key property of the IX dynamics is the radiative lifetime. This radiative lifetime due to the e-h optical recombination is the dominant loss process in such systems, and can in principle be measured directly by time-resolved measurement of the decay of their photoluminescence after a pulse excitation[37–40]. However, as many experiments are done in a steady state under continuous-wave excitation and do not involve a direct lifetime measurement, a method of inferring the lifetime from other measurable quantities can be very useful. In particular, when designing a sample, a complex device, or an experiment, a prior knowledge and understanding of such recombination dynamics could be essential.

Previous theoretical works have proposed various approaches allowing calculation of the lifetime of IXs[41–52]. These have considered some of the sources for the complexity of the general problem, such as the three-dimensional shape of the wavefunction of the bound e-h pair, effect of strong IX localization and other effects. Here we discuss a simpler approach, proposed in our previous work[10], according to which the radiative lifetime of an IX is simply related to its emission energy. This approach disregards many of the aspects addressed by the more general models, limiting its own validity to certain conditions, in order to reach a very simple method to extract lifetimes for IXs. Nevertheless, as we show below, despite its simplicity the model obtained is still expected to be accurate under a wide range of experimentally-accessible parameters.

The model of Ref. 10 considers the recombination lifetime of an IX as being inversely proportional to the squared overlap integral between the envelope wavefunctions of the e and the h along the DQW growth direction z:

$$\tau_{id} = \frac{\tau_d}{|\langle\psi_e|\psi_h\rangle|^2} \tag{1}$$

where τ_{id}, τ_d are the lifetimes of the IX and of the direct exciton (DX), respectively and ψ_e, ψ_h are the envelope

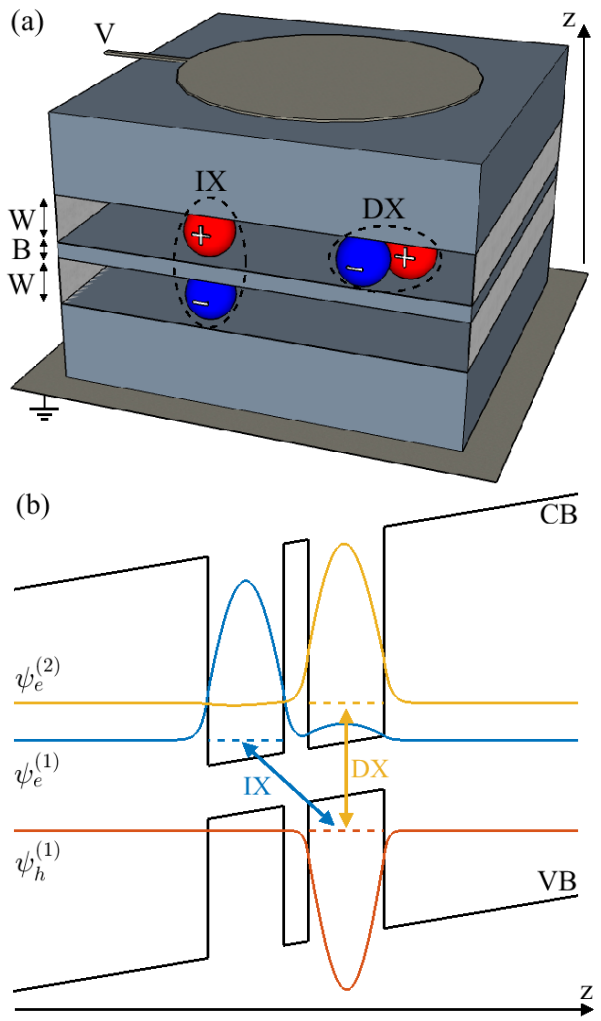

FIG. 1. (a) A simplified illustration of the typical realization of IXs in semiconductor DQW heterostructure. Two quantum wells of width W are separated by a thin central barrier layer marked as B. A metallic gate is positioned on the top of the sample, allowing the induction of electric field in the z direction. Bound pairs of e (blue sphere) and h (red sphere) are created in the wells by optical excitation and can occupy the DX state - where both particles reside in the same well, or in the IX state - where each of them resides in a different well. (b) A typical energy diagram, illustrating the conduction (CB) and valence (VB) energy bands along the z axis, the wavefunctions of the h (red line) and the e occupying the DX (yellow line) and IX (blue line) states, and their corresponding energies (dashed lines). The external electric field is responsible to the tilt of the energy bands, making the IX state lower in energy than the DX state.

wavefunctions of the e and the h along the z-axis, respectively. Fig. 1 schematically illustrates both the DX and IX states in a DQW under an applied electric field along the z-axis.

Under a weak enough external electric field, the envelope wavefunctions of the e and the h in their lowest energy states can be approximated as a linear combination of the corresponding lowest energy flat-band single quantum well (SQW) wavefunctions[53]:

$$\psi_e(z) = c_e^l \psi_e^l(z) + c_e^r \psi_e^r(z) \tag{2a}$$

$$\psi_h(z) = c_h^l \psi_h^l(z) + c_h^r \psi_h^r(z) \tag{2b}$$

Initially, increasing the field will only effect the coefficients and not the validity of the approximation itself. However, when the field becomes strong enough such that the potential drop across each QW is of the order of the difference between the ground energy in the SQW and its first excited state energy, this approximation breaks. Such strong field leads to a substantial admixture of excited states, shifting the peak of each wavefunction away from the tunneling barrier. Another approximation can be made in cases where the effective mass of the h is significantly larger than the effective mass of the e, and under a large enough external field. In such case, the lowest energy h's wavefunction can be well approximated by only one SQW wavefunction, i.e., $\psi_h(z) = \psi_h^r(z)$ in the case of an electric field applied in the positive z-direction, as is illustrated in Fig. 1b. As a result, if the external field is strong enough, the computation of the overlap integral $\langle \psi_e | \psi_h \rangle$ of Eq. 1 can be approximated by integration of the e's wavefunction only inside the right QW, where the h's wavefunction is strongly confined. Thus, there is an intermediate range of electric field values in which both of the above approximations should hold to a good accuracy. Within this range, the computation of the recombination lifetime is reduced to the computation of c_e^r - the amplitude of the e's wavefunction in the h's well:

$$\tau_{id} = \frac{\tau_d}{|c_e^r|^2} \tag{3}$$

As was shown in Ref. 10, the solution of the problem in the basis of ψ_e^l and ψ_e^r yields:

$$c_e^r = \frac{1}{\sqrt{2}} \sqrt{1 - \frac{E_d - E_{id}}{\sqrt{(E_d - E_{id})^2 + 4v_e^2}}}. \tag{4}$$

where E_d and E_{id} are the energies of the DX and IX respectively and v_e is the following tunneling matrix element for the e:

$$v_e = \langle \psi_e^l | (\mathcal{T} + V_e(z)) | \psi_e^r \rangle - \langle \psi_e^l | \psi_e^r \rangle E_0 \tag{5}$$

Here, $\mathcal{T}$ is the kinetic energy, $V_e(z)$ is the DQW potential felt by the electron and E_0 is the ground state energy of a non-interacting electron in a SQW potential. The expression in Eq. 5 is obtained under the assumption that all other contributions to v_e (i.e., the external electric field, the interaction of the electron with neighboring IXs and its coulomb interaction with the h) are negligible. As explained above, Eq. 4 is expected to be valid where the following conditions are satisfied:

$$v_h \ll v_e \tag{6a}$$

$$v_h \ll E_d - E_{id} \ll E_d^{(1)} - E_d^{(0)} \tag{6b}$$

where v_h is the corresponding tunneling matrix element for the h and $E_d^{(n)}$ is the n'th DX energy level in a flat-band SQW. Additionally, in cases where also the following condition is satisfied:

$$v_e \ll \frac{1}{2}(E_d - E_{id}), \tag{7}$$

Eq. 4 is reduced to:

$$c_e^r = \frac{v_e}{E_d - E_{id}}. \tag{8}$$

In such case, the radiative lifetime of an IX can approximately be expressed as[10]:

$$\frac{1}{\tau_{id}} = \frac{1}{\tau_d}\frac{v_e^2}{(E_d - E_{id})^2}. \tag{9}$$

It is worth mentioning the Coulomb binding between the e and the h within an IX. A three-dimensional treatment of the problem shows that the binding energy of an IX may shift due to variation of the external field and the IX-IX interaction, over a few meV's in samples such as that discussed here[48]. This, off course, might have impaired the validity of the discussed model. However, as shown in Appendix A, within the range defined in Eq. 6 this shift is expected to be approximately identical for the DX and the IX, such that its effect on the quantity $E_d - E_{id}$ - and thus also on the accuracy of the model within that range - is negligible.

In this work we numerically test the accuracy and validity limits of Eq. 9 and provide an experimental confirmation of it for a few combinations of experimental parameters which lie within the expected validity range. The structure of this paper is as follows: in Sec. II we compare that analytic result to a numerical calculation using a coupled Schrödinger-Poisson solver under a mean-field approximation of the interactions between IXs. In Sec. III we present experimental results confirming the validity of Eq. 9 and of the underlying approximations. In Sec. IV we summarize our results and their conclusions.

II. COMPARISON TO NUMERICAL CALCULATIONS

To check the validity, accuracy, and applicability limits of Eq. 9, we first compared its predictions with numerical calculations of the overlap between the envelope wavefunctions of the e and the h, using a one-dimensional, self-consistent, Schrödinger-Poisson solver[54]. In the numerical model, we assumed a mean-field approximation for the IX-IX interactions, where in-plane dipolar correlations[9] were neglected, as well as the binding interaction between the e and the h. For any given applied field F and IX density n, we obtained from the solver the envelope wavefunctions for the e and for the h and numerically computed their overlap integral. The IX radiative lifetime is inversely proportional to the square of this overlap integral, and thus it can be calculated up to a multiplicative constant. More importantly, the ratio between the lifetime of the DX and the IX can also be calculated in this way as:

$$\frac{\tau_{id}}{\tau_d} = \frac{\left|\left\langle \psi_e^{(2)} \middle| \psi_h^{(1)} \right\rangle\right|^2}{\left|\left\langle \psi_e^{(1)} \middle| \psi_h^{(1)} \right\rangle\right|^2} \tag{10}$$

where the superscripts mark the corresponding quantum number of the e and h energy levels in the DQW. Substituting Eq. 3 we get the following equation:

$$\frac{\left|\left\langle \psi_e^{(2)} \middle| \psi_h^{(1)} \right\rangle\right|^2}{\left|\left\langle \psi_e^{(1)} \middle| \psi_h^{(1)} \right\rangle\right|^2} = \frac{1}{|c_e^r|^2}. \tag{11}$$

whose r.h.s is determined either by Eq. 4 or by its approximation, Eq. 8. Since the same numerical solver also yields $E_d - E_{id}$, the accuracy of this equality can be used to check the accuracy of Eq. 3, after plugging in the amplitude c_e^r and the e's tunneling matrix element v_e.

The tunneling matrix element v_e can be calculated numerically using the SQW wavefunctions ψ_e^r and ψ_e^l according to Eq. 5 and the h's tunneling matrix element v_h can be calculated similarly. We carried this calculation for the heavy-hole IX in four different realistic GaAs DQW structures: $Al_{0.5}Ga_{0.5}As/GaAs/Al_{0.5}Ga_{0.5}As$ of layer width $W/4nm/W$ differing by their well width W. Their resulted values are presented in Tab. I.

TABLE I. The tunneling matrix element values, for the e and for the hh, in the four DQW structures discussed in Sec. II: $Al_{0.5}Ga_{0.5}As/GaAs/Al_{0.5}Ga_{0.5}As$ of layer width $W/4nm/W$.

W (nm)	8	10	12	14
v_e (meV)	0.33	0.2	0.12	0.08
v_h (meV)	0.003	0.002	0.001	0.0007

The relative error Δ of Eq. 11 is defined as $(r.h.s - l.h.s)/l.h.s$, i.e.

$$\Delta \equiv \frac{1}{|c_e^r|^2} \times \frac{\left|\left\langle \psi_e^{(1)} \middle| \psi_h^{(1)} \right\rangle\right|^2}{\left|\left\langle \psi_e^{(2)} \middle| \psi_h^{(1)} \right\rangle\right|^2} - 1. \tag{12}$$

This error was computed and is presented in Fig. 2a as a function of $E_d - E_{id}$ for the aforementioned four different DQW structures for the single-IX case (i.e. where the IX-IX interaction is set to zero). It is computed both using c_e^r as defined in Eq. 4 (continuous curves) and its first order approximation, Eq. 8 (dashed). The dependence of the relative error Δ on $E_d - E_{id}$ is in agreement with the expected limits of validity mentioned in the previous section: where $E_d - E_{id}$ is very small, the penetration of the

h's wavefunction into the e's QW is significant and using Eq. 4 we get an over-estimation of the radiative lifetime. Once the field is increased such that $E_d - E_{id}$ becomes much larger than v_e, the error drops rapidly and stays low for quite a wide range of $E_d - E_{id}$ values. At even larger values of $E_d - E_{id}$, both the e's and the h's wavefunctions distort in opposite directions and their overlap integral is further diminished. The analytic model does not take this distortion into account (as each of the basis wavefunctions used ψ^l and ψ^r is of a flat bottom QW), and so it underestimates the lifetime, resulting in a relative error which grows with $E_d - E_{id}$ in the negative direction. As expected, this distortion increases with the width of the QWs, leading to a wider $E_d - E_{id}$ range having a high relative accuracy of Eq. 9 for narrower DQWs. Interestingly, the algebric approximation leading from from Eq. 4 to Eq. 8 contributes an error which in low energies is opposite in its sign to the fundamental errors of Eq. 4, as demonstrated in the inset of Fig. 2a. Thus, at low energies the errors tend to cancel each other, making the prediction based on Eq. 8 accurate in a wider range of energies.

Fig. 2b presents the relative error as a function of the IX density n, for a fixed value $E_d - E_{id} = 10$ meV. This is done by setting different values of n and finding the corresponding values of F to keep $E_d - E_{id}$ constant (this method, named 'constant energy line method', was extensively used in our previous experimental works[10,17]). As seen in the figure, the relatively low error values are maintained up to a high IX density of $n \simeq 10^{11}\text{cm}^{-2}$. This demonstrate the robustness of the model also in a multi-particle problem, where the IX-IX interaction may effect E_{id} significantly. Above this density value, the inhomogeneous distribution of the IX charge density along the z-axis of the QWs is large enough to induce large deviations of the e and h wavefunctions from the single-particle wavefunctions, leading to a decrease in the accuracy of the model. In the mean field approximation used here, this can roughly be formulated, using the plate-capacitor formula[9], as the following additional limitation on the validity of the model:

$$\frac{4\pi e^2 dn}{\kappa} \ll E_d^{(1)} - E_d^{(0)} \tag{13}$$

where e is the elementary charge, d is the separation between the centers of the wells and κ is the dielectric constant.

These numerical calculations indicate that Eq. 9 is a good approximation over a significant range of applied electric fields and IX densities and can be tested in experiments, as we show in the next section.

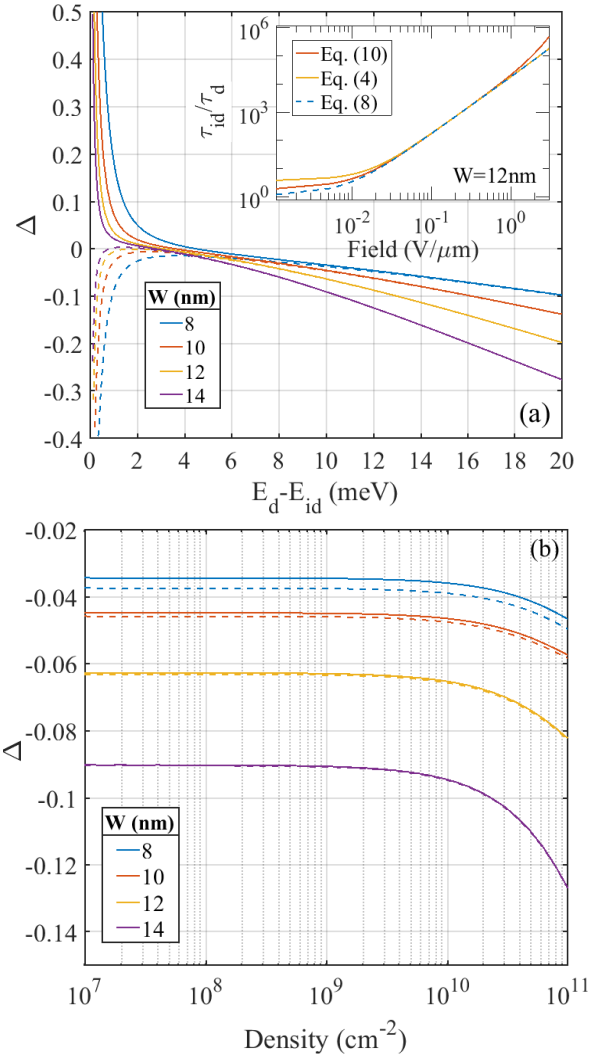

FIG. 2. (a) The relative error Δ of Eq. 11, defined in Eq. 12, plotted against $E_d - E_{id}$ for four different well widths (W) of a $Al_{0.5}Ga_{0.5}As/GaAs/Al_{0.5}Ga_{0.5}As$ DQW structure having tunnling barrier of width $B = 4$nm. It is computed both using Eq. 4 (continuous lines) and using Eq. 8 (dashed lines). The inset demonstrates the source of the calculated values of Δ for the structure where $W = 12$nm, by showing the calculated IX lifetime vs. the external field. The red curve represents the results obtained numerically, according to Eq. 10, the yellow curve represents the lifetimes predicted according to Eq. 8 and the dashed blue curve represents the lifetimes predicted according the further approximated Eq. 8. (b) Δ as a function of the IX density n while the external field is adjusted to keep the constant value of $E_d - E_{id} = 10$ meV, for each of the four DQW structures.

III. COMPARISON TO EXPERIMENTS

A. Experimental Details

The experimental scheme is rather similar to that presented in few of our previous works[10,17]. The sample,

positioned in an optical ^{4}He cryostat, is a 12/4/12nm $Al_{0.5}Ga_{0.5}As/GaAs/Al_{0.5}Ga_{0.5}As$ DQW structure grown on an n^+-doped GaAs substrate and with a 10nm-thick, semi-transparent Ti electrode positioned on its top[17]. The overall thickness of the intrinsic part of the sample is about 1.5μm. An electric field between the top electrode and the doped substrate creates the energy band tilt required for the formation of IXs and allows their trapping as presented in Fig. 3a-b. The sample temperature is maintained at $T = 1.8$K ($\pm 0.1K$).

A population of IXs is being excited using a non-resonant pulsed laser having wavelength of $775nm$ and pulse duration of $300ps$, under a fixed applied electric bias. We then study the decay of the population after the pulse excitation, by time-resolved measurement of the light emitted by recombination of the optically active (i.e 'bright') IXs, using a fast-gated ICCD camera (Princeton Instruments PIMAX).

B. Results

Exemplary time resolved, spatially integrated spectra at different times after the laser excitation are presented in Fig. 3c, for a fixed applied bias of 1V. The spectral lines have a tail to the long wavelength side, similar to previous results. Fig. 3d,e presents the integrated intensity and the IX energy as a function of time after the excitation. The observed redshift during the decay results from the decrease of the interaction energy as the IX density decreases[10].

The radiative recombination of IXs can be described by a simple rate equation:

$$I(t) \propto \frac{\partial n}{\partial t} = \frac{n(t)}{\tau_{id}(t)} \tag{14}$$

where I is the measured emission intensity and τ_{id} is generally time-dependent. Using $n(t) \propto \int_t^\infty I(t')dt'$, and expressing $\tau_{id}(t)$ using Eq. 9 the following relation is obtained:

$$I(t) \propto \frac{\int_t^\infty I(t')dt'}{\left(E_d - E_{id}(t)\right)^2} \equiv G(t) \tag{15}$$

and both $I(t)$ and $G(t)$ can be directly expressed for every t from the experimental results in Fig. 3d,e. The assumptions made in this last derivation are the accuracy of Eq. 9 and that the recombination process is radiatively dominated. Thus, if these assumptions are valid we expect that Eq. 15 should hold for our experimental results, i.e., we expect to find that $G(t) \propto I(t)$ for every t along the whole decay. This is therefore a direct experimental test for Eq. 9.

Fig. 4 presents the experimentally extracted $G(t)$ versus $I(t)$ for four different decay traces that were measured under different external applied biases and laser powers. The solid lines are linear fits to the data. This figure shows early time dynamics, $t < 300$ns, where the density is highest such that the changes in τ_{id} and in E_{id} are most significant. A clear linear dependence appears, which is consistent with the above assumptions and is therefore consistent with Eq. 9.

IV. CONCLUSION

In this work we presented a numerical and experimental test of an approximated derivation relating the IX radiative lifetime to its energy. We showed that this relation is expected to hold well for a wide range of accessible experimental parameters and thus also supported the assumptions used in our previous works[10,17]. We conclude that this relation can be very useful for future works studying IXs in similar bilayer systems, simplifying the analysis of dynamics of IX systems. In many such experiments, the lifetime is a key property whose assessment is not a straight-forward task under the required experimental settings. This difficulty could be relieved by the proposed method, which in principle requires a single calibration measurement to set right the proportion coefficient of Eq. 9 for the sample of interest.

As demonstrated above by the numerical simulation, Eq. 9 is only expected to be valid and accurate enough in an intermediate range of IX energies: The basic picture described by the theoretical model becomes valid only when the separation between the energies of the indirect and the direct excitons is large enough. As the separation is increased further, the accuracy of the model gradually deteriorates and the error of Eq. 9 grows. Between these two ends, lies the range of IX energies where the error is relatively low and Eq. 9 can be used as a good approximation.

We believe that this method can be easily modified for other IX structures that are currently being explored, such as IXs in bilayers of other material systems.

ACKNOWLEDGMENTS

We would like to thank Masha Vladimirova for fruitful discussions. We would also like to acknowledge financial support from the German DFG (grant No. SA-598/9), from the German Israeli Foundation (GIF I-1277-303.10/2014), and from the Israeli Science Foundation (grant No. 1319/12). The work at Princeton University was funded by the Gordon and Betty Moore Foundation through the EPiQS initiative Grant GBMF4420, and by the National Science Foundation MRSEC Grant DMR-1420541.

Appendix A: Exciton Binding

To take the exciton binding into account for the case that the h's tunneling is negligible, one has to solve the

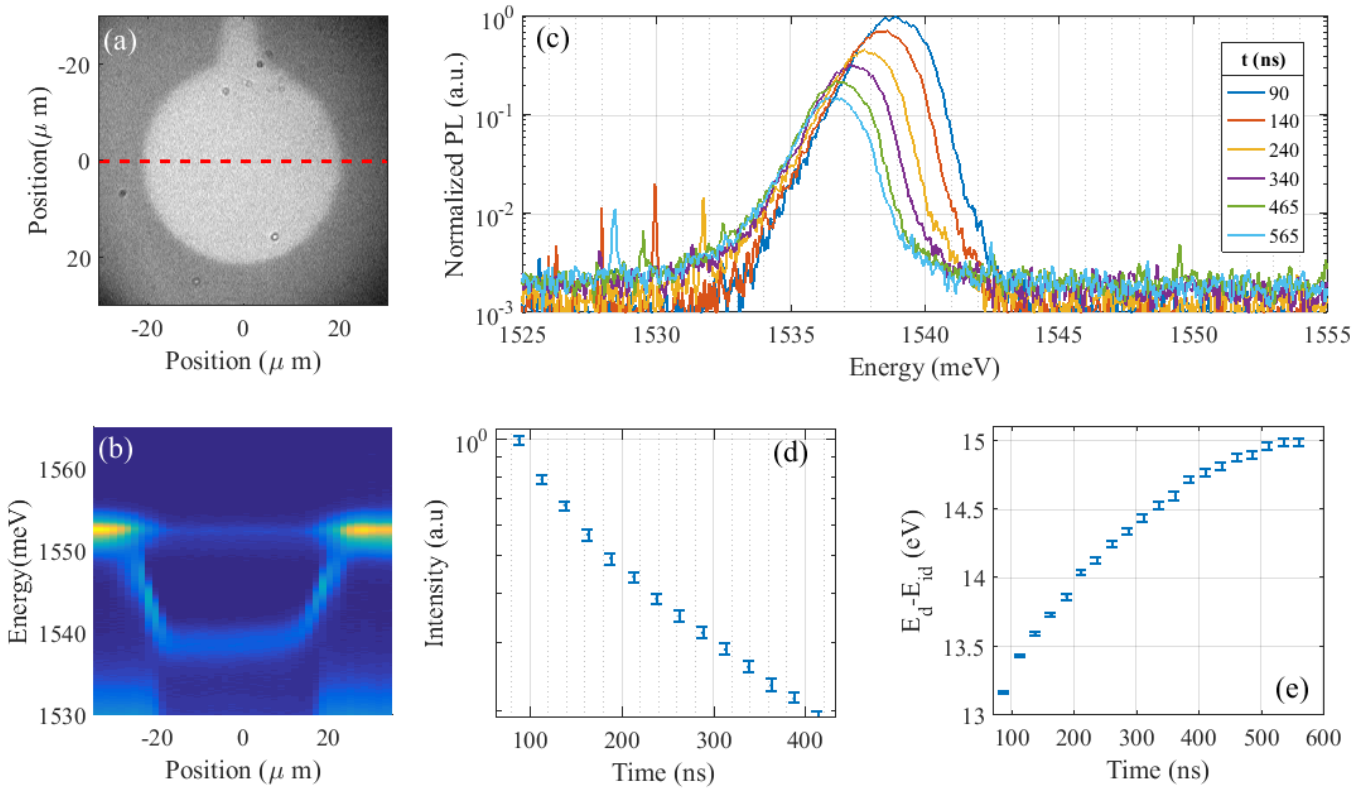

FIG. 3. (a) A real-space image of the circular electrostatic trap used in this work. (b) A spectral-spatial image of the emission from the sample as a function of the position of a CW laser excitation along the dashed red line drawn in (a), with a reversed voltage set to $1V$, an excitation pulse power of 25mW and temperature of $1.8K$. The trapping potential is flat around the center of the trap with $E_d - E_{id} \simeq 12$meV. (c) Exemplary time resolved and spatially integrated spectra at different times after the laser excitation. (d) Integrated intensity I and (e) $E_d - E_{id}$ as a function of time after the laser pulse extracted from the data in (c). All time frames are integrated over a 25ns-wide window.

following 3D Schrödinger equation:

$$-\mathcal{T}\phi^r + \left(U^r - \frac{e^2}{\kappa r}\right)\phi^r + \Gamma\phi^l = E\phi^r \tag{A1a}$$

$$-\mathcal{T}\phi^l + \left(U^l - \frac{e^2}{\kappa\sqrt{r^2+d^2}}\right)\phi^l + \Gamma\phi^r = E\phi^l \tag{A1b}$$

where $\phi \equiv (\phi^r, \phi^l)$ is the wavefunction of the relative position of the e and the h, $\mathcal{T}$ is the kinetic energy, U^r,U^l are the energies above the bottom of each well, $\boldsymbol{r}$ is the in-plane separation between the e and the h, d is the separation between the centers of the wavefunctions of the e and the h in the z direction and Γ is the tunneling energy.

The derivation below does not attempt to obtain a solution for these equations, but rather to use them to estimate the accuracy of the model discussed in the main text, considering the e-h Coloumb binding. For that sake, a spectrum of basis in-plane wavefunctions can be defined by the following Schrödinger equations:

$$-\mathcal{T}\phi_d^{(n)} - \frac{e^2}{\kappa r}\phi_d^{(n)} = -\epsilon_d^{(n)}\phi_d^{(n)} \tag{A2a}$$

$$-\mathcal{T}\phi_{id}^{(n)} - \frac{e^2}{\kappa\sqrt{r^2+d^2}}\phi_{id}^{(n)} = -\epsilon_{id}^{(n)}.\phi_{id}^{(n)} \tag{A2b}$$

The wavefunction (ϕ^l, ϕ^r) can thus be expanded:

$$\phi^r(\boldsymbol{r}) = \sum_n c_d^{(n)}\phi_d^{(n)}(\boldsymbol{r}) \tag{A3a}$$

$$\phi^l(\boldsymbol{r}) = \sum_n c_{id}^{(n)}\phi_{id}^{(n)}(\boldsymbol{r}). \tag{A3b}$$

Substitution of that expansion in Eq.s A2, multiplication by $\phi_d^{(n)}$ and by $\phi_{id}^{(n)}$ and integration in-plane yields the following equations for the coefficients:

$$(U^r + \epsilon_d^{(n)})c_d^{(n)} + \Gamma\sum_{n'}\left\langle\phi_d^{(n)}\middle|\phi_{id}^{(n')}\right\rangle c_{id}^{(n')} = Ec_d^{(n)} \tag{A4a}$$

$$(U^l + \epsilon_{id}^{(n)})c_{id}^{(n)} + \Gamma\sum_{n'}\left\langle\phi_{id}^{(n)}\middle|\phi_d^{(n')}\right\rangle c_d^{(n')} = Ec_{id}^{(n)} \tag{A4b}$$

Under consideration of the ground exciton states ($n = 0$) alone and under the following assumption:

$$\left\langle\phi_d^{(0)}\middle|\phi_{id}^{(n')}\right\rangle \approx \left\langle\phi_d^{(0)}\middle|\phi_{id}^{(0)}\right\rangle\delta_{n',0} \tag{A5a}$$

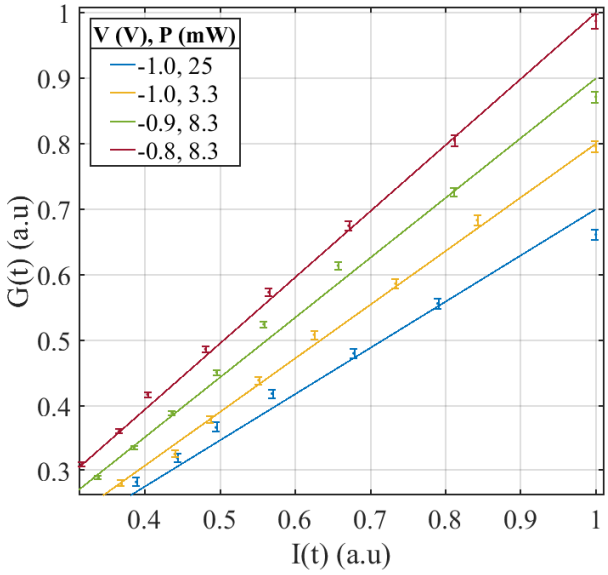

FIG. 4. Experimentally extracted $G(t)$ versus $I(t)$ during $t < 300$ns for four different decay traces that were measured under fixed lattice temperature of $1.8K$ ($\pm 0.1K$) and different combinations of externally applied bias V and laser pulse power P. The solid lines are linear fits to the data. A clear linear dependence is observed, confirming the validity of Eq. 9 for these experimental parameters (The temporal dynamics in each of these measurements is from top-right to bottom-left).

$$\left\langle \phi_{id}^{(0)} \middle| \phi_d^{(n')} \right\rangle \approx \left\langle \phi_{id}^{(0)} \middle| \phi_d^{(0)} \right\rangle \delta_{n',0} \tag{A5b}$$

Eq.s A4 are reduced to:

$$(U^r + \epsilon_d^{(0)}) c_d^{(0)} + \Gamma \left\langle \phi_d^{(0)} \middle| \phi_{id}^{(0)} \right\rangle c_{id}^{(0)} = E c_d^{(0)} \tag{A6a}$$

$$(U^l + \epsilon_{id}^{(0)}) c_{id}^{(0)} + \Gamma \left\langle \phi_d^{(0)} \middle| \phi_{id}^{(0)} \right\rangle c_d^{(0)} = E c_{id}^{(0)}. \tag{A6b}$$

Finally, identifying:

$$E_d = U^r + \epsilon_d^{(0)}, \quad E_{id} = U^l + \epsilon_{id}^{(0)} \tag{A7}$$

and:

$$u = \Gamma \left\langle \phi_d^{(0)} \middle| \phi_{id}^{(0)} \right\rangle = \Gamma \left\langle \phi_{id}^{(0)} \middle| \phi_d^{(0)} \right\rangle, \tag{A8}$$

it is straight-forward to show that Eq.s A6 also lead to the relation of Eq. 4. Thus, even with the exciton binding taken into account, the model and its result of Eq. 9 are valid, limited by the following condition:

$$\left| \left\langle \phi_{id}^{(n)} \middle| \phi_d^{(0)} \right\rangle \right| \ll \left| \left\langle \phi_{id}^{(0)} \middle| \phi_d^{(0)} \right\rangle \right| \tag{A9a}$$

$$\left| \left\langle \phi_{id}^{(0)} \middle| \phi_d^{(n)} \right\rangle \right| \ll \left| \left\langle \phi_{id}^{(0)} \middle| \phi_d^{(0)} \right\rangle \right| \tag{A9b}$$

for every $n > 0$. This condition is roughly the same condition as the r.h.s of Eq. 6b, which implies that as a matter of fact, the model discussed in the main text already accounts for possible variations of the binding energy within the parameters regime where it was shown to be a good approximation.

[1] R. Rapaport and G. Chen, "Experimental methods and analysis of cold and dense dipolar exciton fluids," *Journal of Physics: Condensed Matter*, vol. 19, no. 29, p. 295207, 2007.

[2] L. V. Butov, "Condensation and pattern formation in cold exciton gases in coupled quantum wells," *Journal of Physics: Condensed Matter*, vol. 16, no. 50, p. R1577, 2004.

[3] L. V. Butov, "Cold exciton gases in coupled quantum well structures," *Journal of Physics: Condensed Matter*, vol. 19, no. 29, p. 295202, 2007.

[4] L. V. Butov, A. C. Gossard, and D. S. Chemla, "Macroscopically ordered state in an exciton system," *Nature*, vol. 418, pp. 751–754, Aug. 2002.

[5] D. Snoke, S. Denev, Y. Liu, L. Pfeiffer, and K. West, "Long-range transport in excitonic dark states in coupled quantum wells," *Nature*, vol. 418, pp. 754–757, Aug. 2002.

[6] R. Rapaport, G. Chen, D. Snoke, S. H. Simon, L. Pfeiffer, K. West, Y. Liu, and S. Denev, "Charge Separation of Dense Two-Dimensional Electron-Hole Gases: Mechanism for Exciton Ring Pattern Formation," *Physical Review Letters*, vol. 92, p. 117405, Mar. 2004.

[7] L. V. Butov, L. S. Levitov, A. V. Mintsev, B. D. Simons, A. C. Gossard, and D. S. Chemla, "Formation Mechanism and Low-Temperature Instability of Exciton Rings," *Physical Review Letters*, vol. 92, p. 117404, Mar. 2004.

[8] A. A. High, A. T. Hammack, J. R. Leonard, S. Yang, L. V. Butov, T. Ostatnicky, M. Vladimirova, A. V. Kavokin, T. C. H. Liew, K. L. Campman, and A. C. Gossard, "Spin Currents in a Coherent Exciton Gas," *Physical Review Letters*, vol. 110, p. 246403, June 2013.

[9] B. Laikhtman and R. Rapaport, "Exciton correlations in coupled quantum wells and their luminescence blue shift," *Physical Review B*, vol. 80, p. 195313, Nov. 2009.

[10] Y. Shilo, K. Cohen, B. Laikhtman, K. West, L. Pfeiffer, and R. Rapaport, "Particle correlations and evidence for dark state condensation in a cold dipolar exciton fluid," *Nature Communications*, vol. 4, p. 2335, Aug. 2013.

[11] G. J. Schinner, J. Repp, E. Schubert, A. K. Rai, D. Reuter, A. D. Wieck, A. O. Govorov, A. W. Holleitner, and J. P. Kotthaus, "Confinement and Interaction of Single Indirect Excitons in a Voltage-Controlled Trap Formed Inside Double InGaAs Quantum Wells," *Physical Review Letters*,

vol. 110, p. 127403, Mar. 2013.

[12] K. Cohen, M. Khodas, B. Laikhtman, P. V. Santos, and R. Rapaport, "Vertically coupled dipolar exciton molecules," *Physical Review B*, vol. 93, p. 235310, June 2016.

[13] L. V. Butov, C. W. Lai, A. L. Ivanov, A. C. Gossard, and D. S. Chemla, "Towards Bose-Einstein condensation of excitons in potential traps," *Nature*, vol. 417, pp. 47–52, May 2002.

[14] M. Combescot, O. Betbeder-Matibet, and R. Combescot, "Bose-Einstein Condensation in Semiconductors: The Key Role of Dark Excitons," *Physical Review Letters*, vol. 99, p. 176403, Oct. 2007.

[15] M. Alloing, M. Beian, M. Lewenstein, D. Fuster, Y. González, L. González, Combescot, R., M. Combescot, and F. Dubin, "Evidence for a Bose-Einstein condensate of excitons," *EPL (Europhysics Letters)*, vol. 107, no. 1, p. 10012, 2014.

[16] M. Stern, V. Umansky, and I. Bar-Joseph, "Exciton Liquid in Coupled Quantum Wells," *Science*, vol. 343, pp. 55–57, Jan. 2014.

[17] K. Cohen, Y. Shilo, K. West, L. Pfeiffer, and R. Rapaport, "Dark High Density Dipolar Liquid of Excitons," *Nano Letters*, vol. 16, pp. 3726–3731, June 2016.

[18] R. Rapaport, G. Chen, S. Simon, O. Mitrofanov, L. Pfeiffer, and P. M. Platzman, "Electrostatic traps for dipolar excitons," *Physical Review B*, vol. 72, p. 075428, Aug. 2005.

[19] A. T. Hammack, M. Griswold, L. V. Butov, L. E. Smallwood, A. L. Ivanov, and A. C. Gossard, "Trapping of Cold Excitons in Quantum Well Structures with Laser Light," *Physical Review Letters*, vol. 96, p. 227402, June 2006.

[20] K. Kowalik-Seidl, X. P. Vögele, B. N. Rimpfl, G. J. Schinner, D. Schuh, W. Wegscheider, A. W. Holleitner, and J. P. Kotthaus, "Tunable Photoemission from an Excitonic Antitrap," *Nano Letters*, vol. 12, pp. 326–330, Jan. 2012.

[21] M. Alloing, A. Lemaître, E. Galopin, and F. Dubin, "Optically programmable excitonic traps," *Scientific Reports*, vol. 3, Apr. 2013.

[22] A. A. High, E. E. Novitskaya, L. V. Butov, M. Hanson, and A. C. Gossard, "Control of Exciton Fluxes in an Excitonic Integrated Circuit," *Science*, vol. 321, pp. 229–231, July 2008.

[23] A. Violante, K. Cohen, S. Lazic, R. Hey, R. Rapaport, and P. V. Santos, "Dynamics of indirect exciton transport by moving acoustic fields," *New Journal of Physics*, vol. 16, no. 3, p. 033035, 2014.

[24] A. G. Winbow, J. R. Leonard, M. Remeika, Y. Y. Kuznetsova, A. A. High, A. T. Hammack, L. V. Butov, J. Wilkes, A. A. Guenther, A. L. Ivanov, M. Hanson, and A. C. Gossard, "Electrostatic Conveyer for Excitons," *Physical Review Letters*, vol. 106, p. 196806, May 2011.

[25] K. Cohen, R. Rapaport, and P. V. Santos, "Remote Dipolar Interactions for Objective Density Calibration and Flow Control of Excitonic Fluids," *Physical Review Letters*, vol. 106, p. 126402, Mar. 2011.

[26] S. Lazić, A. Violante, K. Cohen, R. Hey, R. Rapaport, and P. V. Santos, "Scalable interconnections for remote indirect exciton systems based on acoustic transport," *Physical Review B*, vol. 89, p. 085313, Feb. 2014.

[27] J. R. Leonard, Y. Y. Kuznetsova, S. Yang, L. V. Butov, T. Ostatnický, A. Kavokin, and A. C. Gossard, "Spin Transport of Excitons," *Nano Letters*, vol. 9, pp. 4204–4208, Dec. 2009.

[28] K. Kowalik-Seidl, X. P. Vögele, B. N. Rimpfl, S. Manus, J. P. Kotthaus, D. Schuh, W. Wegscheider, and A. W. Holleitner, "Long exciton spin relaxation in coupled quantum wells," *Applied Physics Letters*, vol. 97, p. 011104, July 2010.

[29] P. Rivera, J. R. Schaibley, A. M. Jones, J. S. Ross, S. Wu, G. Aivazian, P. Klement, K. Seyler, G. Clark, N. J. Ghimire, J. Yan, D. G. Mandrus, W. Yao, and X. Xu, "Observation of long-lived interlayer excitons in monolayer MoSe2-WSe2 heterostructures," *Nature Communications*, vol. 6, p. 6242, Feb. 2015.

[30] P. Rivera, K. L. Seyler, H. Yu, J. R. Schaibley, J. Yan, D. G. Mandrus, W. Yao, and X. Xu, "Valley-polarized exciton dynamics in a 2d semiconductor heterostructure," *Science*, vol. 351, pp. 688–691, Feb. 2016.

[31] J. I. A. Li, T. Taniguchi, K. Watanabe, J. Hone, A. Levchenko, and C. R. Dean, "Negative Coulomb Drag in Double Bilayer Graphene," *Physical Review Letters*, vol. 117, p. 046802, July 2016.

[32] J. I. A. Li, T. Taniguchi, K. Watanabe, J. Hone, and C. R. Dean, "Excitonic superfluid phase in Double Bilayer Graphene," *arXiv:1608.05846 [cond-mat]*, Aug. 2016. arXiv: 1608.05846.

[33] P. Cristofolini, G. Christmann, S. I. Tsintzos, G. Deligeorgis, G. Konstantinidis, Z. Hatzopoulos, P. G. Savvidis, and J. J. Baumberg, "Coupling Quantum Tunneling with Cavity Photons," *Science*, vol. 336, pp. 704–707, May 2012.

[34] I. Rosenberg, Y. Mazuz-Harpaz, R. Rapaport, K. West, and L. Pfeiffer, "Electrically controlled mutual interactions of flying waveguide dipolaritons," *Physical Review B*, vol. 93, p. 195151, May 2016.

[35] J. Wilkes and E. A. Muljarov, "Dipolar polaritons in microcavity-embedded coupled quantum wells in electric and magnetic fields," *Physical Review B*, vol. 94, p. 125310, Sept. 2016.

[36] V. Shahnazaryan, O. Kyriienko, and I. A. Shelykh, "Adiabatic preparation of a cold exciton condensate," *Physical Review B*, vol. 91, p. 085302, Feb. 2015.

[37] C. C. Phillips, R. Eccleston, and S. R. Andrews, "Theoretical and experimental picosecond photoluminescence studies of the quantum-confined Stark effect in a strongly coupled double-quantum-well structure," *Physical Review B*, vol. 40, pp. 9760–9766, Nov. 1989.

[38] J. E. Golub, K. Kash, J. P. Harbison, and L. T. Florez, "Long-lived spatially indirect excitons in coupled GaAs/Al x Ga 1- x As quantum wells.," *Physical Review B*, vol. 41, pp. 8564–8567, Apr. 1990.

[39] A. Alexandrou, J. A. Kash, E. E. Mendez, M. Zachau, J. M. Hong, T. Fukuzawa, and Y. Hase, "Electric-field effects on exciton lifetimes in symmetric coupled GaAs/Al 0.3 Ga 0.7 As double quantum wells.," *Physical Review B*, vol. 42, pp. 9225–9228, Nov. 1990.

[40] S. Charbonneau, M. L. W. Thewalt, E. S. Koteles, and B. Elman, "Transformation of spatially direct to spatially indirect excitons in coupled double quantum wells," *Physical Review B*, vol. 38, pp. 6287–6290, Sept. 1988.

[41] I. Galbraith and G. Duggan, "Exciton binding energy and external-field-induced blue shift in double quantum wells," *Physical Review B*, vol. 40, pp. 5515–5521, Sept. 1989.

[42] T. Kamizato and M. Matsuura, "Excitons in double quantum wells," *Physical Review B*, vol. 40, pp. 8378–8384, Oct. 1989.

[43] J. Lee, M. O. Vassell, E. S. Koteles, and B. Elman, "Excitonic spectra of asymmetric, coupled double quantum wells

in electric fields," *Physical Review B*, vol. 39, pp. 10133–10143, May 1989.

[44] M. M. Dignam and J. E. Sipe, "Exciton states in coupled double quantum wells in a static electric field," *Physical Review B*, vol. 43, pp. 4084–4096, Feb. 1991.

[45] I. Linnerud and K. A. Chao, "Exciton binding energies and oscillator strengths in a symmetric Al x Ga 1-x As/GaAs double quantum well.," *Physical Review B*, vol. 49, pp. 8487–8490, Mar. 1994.

[46] Y. Takahashi, Y. Kato, S. S. Kano, S. Fukatsu, Y. Shiraki, and R. Ito, "The effect of electric field on the excitonic states in coupled quantum well structures," *Journal of Applied Physics*, vol. 76, pp. 2299–2305, Aug. 1994.

[47] J. Soubusta, R. Grill, P. Hlidek, M. Zvara, L. Smrcka, S. Malzer, W. Geisselbrecht, and G. H. Dohler, "Excitonic photoluminescence in symmetric coupled double quantum wells subject to an external electric field," *Physical Review B*, vol. 60, pp. 7740–7743, Sept. 1999.

[48] M. H. Szymanska and P. B. Littlewood, "Excitonic binding in coupled quantum wells," *Physical Review B*, vol. 67, p. 193305, May 2003.

[49] S. C. Arapan and M. A. Liberman, "Exciton levels and optical absorption in coupled double quantum well structures," *Journal of Luminescence*, vol. 112, pp. 216–219, Apr. 2005.

[50] K. Sivalertporn, L. Mouchliadis, A. L. Ivanov, R. Philp, and E. A. Muljarov, "Direct and indirect excitons in semiconductor coupled quantum wells in an applied electric field," *Physical Review B*, vol. 85, p. 045207, Jan. 2012.

[51] D. S. Citrin, "Radiative lifetimes of excitons in quantum wells: Localization and phase-coherence effects," *Physical Review B*, vol. 47, pp. 3832–3841, Feb. 1993.

[52] K. Sivalertporn, "Effect of barrier width on the exciton states in coupled quantum wells in an applied electric field," *Physics Letters A*, vol. 380, pp. 1990–1994, May 2016.

[53] G. Bastard, *Wave mechanics applied to semiconductor heterostructures*. Monographies de physique, Les Ulis Cedex, France : New York, N.Y: Les Editions de Physique ; Halsted Press, 1988.

[54] P. Harrison, *Quantum wells, wires, and dots: theoretical and computational physics*. Chichester ; New York: Wiley, 2000.